High b-value and diffusion tensor imaging in a canine model of dysmyelination and brain maturation

Yu-Chien Wu[a,b,c], **Aaron S. Field**[a,d], **Ian D. Duncan**[e], **Alexey A Samsonov**[a], **Yoichi Kondo**[e], **Dana Tudorascu**[b], and **Andrew L. Alexander**[b,f,g]

[a]Department of Radiology, University of Wisconsin-Madison, Madison, WI, USA

[b]Waisman Laboratory for Brain Imaging and Behavior, University of Wisconsin-Madison, Madison, WI, USA

[c]Dartmouth Brain Imaging Center, Dartmouth College, Hanover, NH, USA

[d]Department of Biomedical Engineering, University of Wisconsin-Madison, Madison, WI, USA

[e]Department of Medical Sciences, School of Veterinary Medicine, University of Wisconsin-Madison, Madison, WI, USA

[f]Department of Medical Physics, University of Wisconsin-Madison, Madison, WI, USA

[g]Department of Psychiatry, University of Wisconsin-Madison, Madison, WI, USA

Abstract

Recent studies in rodents have demonstrated that diffusion imaging is highly sensitive to differences in myelination. These studies suggest that demyelination/dysmyelination cause increases in the radial diffusivity from diffusion tensor imaging (DTI) measurements and decreases in the restricted diffusion component from high b-value diffusion-weighted imaging experiments. In this study, the *shaking* pup (*sh* pup), a canine model of dysmyelination, was studied on a clinical MRI scanner using a combination of conventional diffusion tensor imaging and high b-value diffusion-weighted imaging methods. Diffusion measurements were compared between control dogs and *sh* pups in the age range 3 months to 16 months, which is similar to the period of early childhood through adolescence in humans. The study revealed significant group differences in nearly all diffusion measures with the largest differences in the zero-displacement probability (Po) from high b-value DWI and the radial diffusivity from DTI, which are consistent with the observations from the published rodent studies. Age-related changes in Po, FA, mean diffusivity, radial diffusivity and axial diffusivity were observed in whole brain white matter for the control dogs, but not the *sh* pups. Regionally, age-related changes in the *sh* pup white matter were observed for Po, mean diffusivity and radial diffusivity in the internal capsule, which may be indicative of mild myelination. These studies demonstrate that DWI may be used to study myelin abnormalities and brain development in large animal models on clinical MRI scanners, which are more amenable to translation to human studies.

Introduction

Quantitative imaging measures that are both sensitive and specific to white matter (WM) pathophysiology would be extremely valuable. Imaging biomarkers of myelin, in particular, would be extremely helpful for diagnosing, characterizing and monitoring many diseases of the central nervous system including multiple sclerosis (MS) and amyotrophic lateral sclerosis (ALS). Myelin biomarkers would also be a powerful way of characterizing myelin changes throughout the lifespan, particularly during brain development and maturation.

Magnetic resonance diffusion tensor imaging (DTI) is widely used for the study of WM diseases. DTI is non-invasive and can be performed in a relatively short scan time that is acceptable for the clinical setting. The diffusion tensor may be used to characterize the microstructural features of brain tissues, although the model is limited by its assumption of a Gaussian distribution of water diffusion (Basser 1994, 1996). The mean diffusivity (MD) is inversely related to the density of the tissue membranes and the fractional anisotropy (FA) describes the degree of local coherence of white matter fiber bundles (Beaulieu and Allen 1994; Ono et al 1995). Recent rodent model studies have suggested that decreases in the axial diffusivity (Da) of the diffusion tensor may reflect axonal degeneration, whereas increased radial diffusivity (Dr) appears to be more specific to demyelination (Song S-K 2002; Tyszka et al., 2006; Harsan et al., 2006, 2007). DTI has been widely used to study diseases that cause demyelination like MS (Ge et al., 2005; Sundgren et al., 2004; Henry et al., 2009) including using the axial and radial diffusivities to characterize axonal and myelin changes, respectively (Henry et al., 2003; Kim et al., 2006; Budde et al., 2008). DTI has also been used to characterize developmental brain changes through childhood and adolescence in humans (Miller et al., 2003; Suzuki et al., 2003; Berman et al., 2005; Hermoye et al., 2006; Elunvathingal et al., 2007; Davis et al., 2009), as well as postnatal brain development in mice (Zhang et al., 2005), rats (Bockhorst et al., 2008), cats (Baratti et al., 1999), and rabbits (D'Arceuil et al., 2008).

However, it has been observed that DTI measures are highly sensitive to several confounds including non-Gaussian diffusion, crossing fibers and imaging noise (Mulkern et al., 1999; Alexander et al., 2001; Pierpaoli and Basser, 1996). As alternatives to DTI, q-space imaging and diffusion spectrum imaging (DSI) may provide more accurate measurements of complex WM microstructure. The q-space formalism was first introduced by Callaghan (Callaghan, 1991), and recently DSI, an adaptation of this approach on clinical scanners, has been applied to diffusion imaging of the human brain (Wu and Alexander, 2007, Wedeen et al., 2005, Assaf et al., 2002). DSI acquires diffusion-weighted (DW) images at multiple DW directions as well as multiple DW strengths up to moderately high b-values. The DSI approach does not assume any specific model of water diffusion and allows the diffusion distribution (probability density function – PDF) to be directly estimated. The zero displacement probability (Po) of the PDF is a scalar measure describing the degree of water restriction in the tissue (Assaf et al., 2002, Wu and Alexander, 2007), which appears to be decreased in the normal appearing white matter of patients with MS (Assaf et al., 2002). Recent studies in myelin deficient rat spinal cord and brain have shown significant changes in q-space measures at high diffusion-weighting (b-values) apparently corresponding to myelin (Bar-Shir et al., 2009). Other studies have used q-space imaging methods (including

DSI) to study brain development in children (Ben Bashat et al., 2005) and cats (Takahashi et al., 2010).

An adaptation of DSI is hybrid diffusion imaging (HYDI), which uses a non-Cartesian q-space encoding scheme, which consists of several concentric spherical shells (Wu and Alexander, 2007; Wu et al., 2008). The flexibility of this scheme facilitates the application of multiple data analyses including DTI (reconstructed from inner shells) and DSI (reconstructed from whole dataset). In this study, HYDI was used to investigate the effects of myelination and brain maturation in the *shaking* (*sh*) pup canine model of dysmyelination. The *sh* pup has a point mutation in the myelin proteolipid protein (PLP) gene leading to profound hypomyelination (Nadon et al., 1999) and is a large animal model of the human X-linked leukodystrophy Pelizaeus-Merzbacher Disease (PMD), an X-linked leukodystrophy, in humans. The WM in the *sh* pup model is diffusely and markedly myelin-deficient, but axons are largely preserved, making this an excellent model for studying the effects of myelin on quantitative imaging without the confounding effects of axonal loss, inflammation or edema, which are common confounders in inflammatory demyelinating models like EAE. Diffusion MRI abnormalities in PMD have been reported in several imaging studies since 1994 (Ono et al., 1994 & 1997; Sener, 2004; Miller et al., 2010). One strength of this model is that it is a large animal that can be characterized using clinical MRI scanners and conventional pulse sequences; thus the potential for translation to humans is high. HYDI measurements were obtained in both *sh* pup and control animals over a range of ages (3–16 months), which also permitted the characterization of microstructural changes over a period of brain maturation. It was expected that the control dogs would demonstrate white matter myelination over this age period, whereas the myelin related changes in the *sh* pup would be minimal. This reductionist disease model may help to disentangle the many confounding pathological changes that occur in MS and other WM diseases and relate them to changes in diffusion properties observable with MR.

Materials and Methods

Animal

For the cohort study, seven *sh* pups and six control littermates were scanned 1, 2 or 3 times at roughly three-month intervals. The ages of the dogs ranged between 3 and 45.6 months for control dogs and between 3 and 21 months for *sh* pups (average life span for *sh* pups is ~24 months). During the MR scans, the animals were intubated and anesthetized using isofluorene. The protocol was approved and performed under the guidelines of the university animal welfare board (IACCUC). During the scans vital signs were closely monitored by a veterinary anesthesia technologist inside the scanner room.

HYDI Acquisition

Quantitative MR experiments were performed on a 3T GE SIGNA whole body scanner (GE Healthcare, Waukesha, WI) with a quadrature extremity coil. HYDI was performed using a diffusion-weighted, single-shot, spin-echo, EPI (SS-SE-EPI) sequence. The HYDI sampling scheme listed in Table 1 consisted of four concentric shells. The maximum b-value was 6500 s/mm^2 with a maximum diffusion-weighting (DW) gradient of 40 mT/m and gradient duration (δ) and separation (Δ) of 39 and 50 ms, respectively. This sampling scheme corresponded to $\Delta q_r = 16.1$ mm^{-1} and maximum q = 64.9 mm^{-1} (Table 1). The field of view ($FOV_R = (\Delta q_r)^{-1}$) and the resolution ($(2*q_{r,max})^{-1}$) of the displacement distribution function were 46 μm and 7.7 μm, respectively. MR images had an in-plane resolution = 1.56 mm (FOV=150 mm and matrix size = 96×96) interpolated to 0.59 mm voxels, 26 contiguous 'coronal' slices with slice thickness = 3 mm from the upper cervical cord to the olfactory bulb. The TE/TR= 130/7500 ms and the total scanning time was approximately 30 minutes.

HYDI Data Processing

The second shells of the HYDI acquisition in Table 1 were used for DTI processing and the entire dataset was used for diffusion spectrum processing. DTI measures were post-processed using Camino software (Cook et al., 2006) including fractional anisotropy (FA), mean diffusivity (MD), axial diffusivity (Da), and radial diffusivity (Dr), where Da is the major eigenvalue of the diffusion tensor (DT) and Dr is the average of the medium and minor eigenvalues of DT. The diffusion spectrum was processed using in-house Matlab software as described by Wu et al. (Wu et al., 2008). The diffusion probability density function (PDF) was summarized using the zero displacement probability, Po, which is a measure of restricted diffusion. In the healthy adult brain, Po is greater in white matter (WM) than gray matter (GM) because WM has more restricting barriers including multi-layer myelin sheaths, axonal membranes, and the microtubules (cytoskeleton). The Po measure appears to be relatively insensitive to WM fiber crossings, which cause reductions in the fractional anisotropy (FA) of DTI.

Brain extraction using manual tracing methods was performed on the MR images prior to image analysis. WM tissues were segmented by two-stage segmentation using the FAST algorithm (Zhang et al., 2001) in the FSL toolbox developed by FMRIB (Oxford Center for Functional MRI of the Brian). First, a 2-class segmentation was done on MD to separate CSF from parenchyma. Second, a 2-class segmentation was done using FA to separate WM and GM. FA was hyperintense in WM for both control and *sh* pup animals, which made it the best candidate for segmentation. This segmentation approach, which did not rely on predefined FA and MD thresholds, generated consistent white matter masks for all animals in both groups. To obtain more anatomically specific measurements, manual ROI analyses were also performed at the bilateral internal capsules (IC) and bilateral caudate nuclei (CN). The former is intended to specifically assess a large region of compact white matter and the latter is to evaluate deep brain gray matter. Diffusion measures of WM were compared between controls and *sh* pups and characterized across the age range.

Statistical Analyses

All the DW measures of both whole brain WM and ROIs were regressed on age using nonlinear and linear regression analyses with the weighted least square (WLS) method. The nonlinear model is

$$\text{DW} - \text{measures} = \beta_2{}^*\exp(\beta_1{}^*\text{age}) + \beta_0 + \text{noise}, \tag{1}$$

and the linear model is

$$\text{DW} - \text{measures} = \beta_1{}^*\text{age} + \beta_0 + \text{noise}. \tag{2}$$

For the linear regression, only scans between 3 and 16 months were considered because this age range represents a period of relatively rapid brain maturation (roughly equivalent to infancy through adolescence in humans), as evidenced by a plateau in the age-related diffusion changes observed at ~16 months in normal dogs. The linear models were compared between *sh* and control pups and were tested using ANOVAs. Statistical significance was assessed at a p-value less than 0.05.

Results

The geometric means of diffusion-weighted signals at different levels of diffusion weighting are depicted in Figure 1. The contrast between gray matter (GM) and white matter (WM) appears quite different for all levels of diffusion-weighting. At high diffusion-weighting the WM of the control pup still had significant signal, which was absent in the *sh* pup.

Typical HYDI maps (i.e. Po) and DTI maps (i.e. FA, MD, Da, Dr) for a *sh* pup and a control dog are shown in Figure 2. In the control dog, Po is clearly greater in WM, which was not true for the *sh* pup. The Dr of WM is also obviously increased in the *sh* pup. The appearances of the contrast for the FA, MD and Da maps are similar for both groups. This supports previous observations that ordered axonal structures yield anisotropic diffusion even in the absence of myelin. The relatively preserved gray-white contrast on FA maps of *sh* pups relative to controls was useful for segmenting the WM.

Most diffusion measures demonstrated highly significant group differences in WM when all ages were considered together (Table 2). Po showed the greatest relative group difference in WM (37–45% decrease in *sh* pup), followed by Dr, FA, and MD and finally Da. In the caudate nucleus (CN), Po, MSD, FA and Da were all significantly reduced in the *sh* pup although the effect size was smaller than in WM.

The age and group effects on the diffusion measures are summarized in Figures 3–6 and for whole-brain WM (WBWM) and bilateral regions-of-interest (ROIs) in the internal capsules (IC) and caudate nuclei (CN). The nonlinear model fit the main developmental changes in Po for the control dogs in WM (both WB [Po=−0.32*exp(−0.197*age)+0.562] and IC ROI [Po=−0.353*exp(−0261*age)+0.635]), where Po increased rapidly over the first 10 months and then plateaued at around 11–15 months (Figure 3). The nonlinear model was not significant for the other measures in controls. We did not have measurements at older ages (>16 mo) in the *sh* pups to characterize nonlinear aging effects in that group.

For WBWM up to 16 months, the linear model showed significant age-related increases in Po and FA, and decreases in MD, Da, and Dr in the control dogs, but not the *sh* pups (Figure 4). The estimated parameters of linear model for the IC ROI are listed in Table 3. In the IC ROI (Table 3 and Figure 5), Po significantly increased with age and both MD and Dr decreased with age for both *sh* pups and control dogs. The age-related change in Po was significantly greater for the control dogs than in the *sh* pups (p=0.0457); however, the slopes of MD or Dr were not significantly different between groups (Table 3). FA and Da did not show significant age-related changes for either group. Interestingly in the CN (Figure 6), the control dogs demonstrated a significant increase in Po and decreases in MD and Dr with age.

Discussion

In this study, a large-animal dysmyelination model, the *sh* pup, was used to investigate the sensitivity of high b-value diffusion imaging to the presence of myelin in white matter. Significant group differences in both WBWM and internal capsule WM were observed for most of the measures. Both the Po and Dr measures showed the largest relative group differences (Table 2). The increased radial diffusivity, Dr, measurements in the *sh* pups are consistent with studies in dysmyelination models like the shiverer mouse and the jimpy mouse (Song et al., 2002; Tyszka et al., 2006; Harsan et al., 2006, 2007), the myelin deficient (*md*) rat brain and spinal cord (Biton et al., 2007; Bar-Shir et al., 2009), and with abnormal diffusion anisotropy reported in humans with PMD (Ono et al., 1994 & 1997; Sener 2004; Miller et al., 2010). It is believed that Dr is a fairly specific biomarker of myelin (Song et al., 2002) although its validity in regions of complex crossing WM has been

questioned (Wheeler-Kingshot and Cercignani, 2009). Increased axial diffusivity, Da, in white matter was also observed in this study (Table 2), which is consistent with observations in fixed, post-mortem spinal cord and brain specimens from the *md* rat (Biton et al., 2007, Bar-Shir et al., 2009) and the jimpy mouse white matter *in vivo* (Harsan et al., 2007). However, these observations are inconsistent with the reported lack of Da changes by Song et al. (2002) in the shiverer mouse model of dysmyelination. It is has been assumed that axial diffusivity differences are associated with axonal changes (Kim et al., 2006; Harsan et al., 2007); though this hypothesis is based upon models of brain injury (Sun et al., 2006) and may not reflect abnormalities in brain development. Consequently, the specific mechanism for Da changes remains unclear.

The results for the high b-value HYDI data demonstrated significantly reduced restricted diffusion, Po, in the sh pup, consistent with previous q-space measurements in fixed tissue specimens from the *md* rat brain and spinal cord (Biton et al., 2007; Bar-Shir et al. 2009). These studies suggest that changes in myelin are the primary mechanism for the differences in Po. These studies also examined the effects of diffusion time on the measurements in both the *md* rat and control animals. The brain study revealed no significant group differences in mean displacements for 'short' diffusion times (40 ms) but significantly reduced displacements for diffusion times of 100 ms or longer. However, in fixed spinal cord with short diffusion times (40–50 ms), the same group has reported significant reductions in Po for the md rat (Biton et al., 2006; 2007). Direct comparisons with the studies in the *md* rat are limited by the differences in the tissue (*in vivo* versus fixed) and the diffusion imaging parameters (wide diffusion pulses versus narrow pulses).

Another potential mechanism for the reduced Po in the *sh* pup white matter may be differences in the axons as well. Researchers have hypothesized that the restricted diffusion signal at high b-values primarily originates from the intra-axonal compartment (Assaf and Cohen 2000; Assaf and Basser 2005), which is supported by recent, elegant studies of axonal diameter both *ex vivo* and *in vivo* (Assaf et a. 2008; Barazany et al., 2009). Reductions in the axonal diameter have been reported in jimpy mice with white matter dysmyelination (Harsan et al., 2006). The water permeability between the intra- and extra-axonal spaces may also be increased in the case of unmyelinated axons, which may decrease the amount of restricted diffusion. There are other cell types (oligodendrocytes, astrocytes) and membranes (intracellular, vascular) in the white matter which could also influence diffusion and be affected in the *sh* pup.

In the control sample, an age-related plateau was observed in white matter Po starting at around 12–16 months (Fig. 3). In the 3 – 16 months age range, the whole brain white matter showed linear changes in all the diffusion measures in controls, but not *sh* pups (Fig. 4). These linear age-related changes are consistent with age-related DTI changes in humans up through adolescence (Miller et al., 2003; Suzuki et al., 2003; Berman et al., 2005; Hermoye et al., 2006; Elunvathingal et al., 2007; Davis et al., 2009). These developmental changes in diffusion measures may reflect a combination of myelination, increased axonal density, and/ or increased axonal diameters. For the measurements in the internal capsule (Fig. 5), Po, MD and Dr (but not FA or Da) showed significant age-related changes for both controls and *sh* pups although, for Po, the age effects were significantly larger in the control. The radial diffusivity changes in the internal capsule of the *sh* pups may reflect myelination changes with age. Although the *sh* pups are clearly less myelinated than the control dogs, they do develop some myelin. The group differences in the diffusion measures appeared to be consistent across the range of ages examined.

Another interesting observation is that in the region of gray matter that was evaluated, several of the diffusion measures (Po, FA and Da) were also abnormal in the *sh* pup sample

including differences in the developmental trajectories of Po, MD, and Dr (Fig. 6). These differences suggest that the disease process in *sh* pups is not limited to the white matter.

The profound differences in white matter myelination of the brain between representative control and *sh* pup dogs are illustrated in Fig. 7. Histologic myelin staining shows reversal of contrast between white matter and gray matter in the *sh* pup. Light microscopy of internal capsule cross-sections confirmed similar axonal distributions in both control (2 year old) and *sh* pups (~1 month old), but significantly less myelin in the *sh* pups. Myelination slightly increased in the *sh* pup with age (Fig. 7(d) to (f)), though the axons remained much less myelinated than the control dogs (Fig. 7(c) and (e)). These group differences and age-related changes are consistent with the trends observed for the Po and Dr measurements in the internal capsule for our sample (Fig 5). Previous published studies that compared the CNS development of *sh* pups with wild type (control) dogs reported some increased myelination (but much reduced relative to the wild type) in the brain and spinal cord of the *sh* pup with age, though this was only studied up to 10 weeks in the brain but out to 2 years in the cord (Griffiths et al., 1981; Nadon and Duncan, 1996). This hypomyelination is caused by a point mutation in the myelin proteolipid protein (PLP) gene that inhibits the development of mature oligodendrocytes (Nadon et al., 1990) and reduces the production of myelin proteins (PLP and myelin basic protein) in the *sh* pup (Nadon and Duncan 1996). Other glia including astrocytes appear unaffected. These myelin deficits are more representative of dysmyelination rather than demyelination as there is no evidence of myelin debris or inflammation. Despite the significant hypomyelination, the distribution of axonal diameters in the *sh* pup appears similar to the wild type (Duncan et al. 1983) though this has not been quantitatively characterized.

Both DSI (HYDI) and DTI measures Po and Dr, respectively, demonstrated significant sensitivity to both group and age maturation effects, which suggests that both approaches may be useful for characterizing myelin differences in human populations. DTI is now widely available on most clinical MRI scanners and its application in clinical and research studies are rapidly growing. The acquisition of DTI data is fairly rapid (on the order of 5–10 minutes for whole brain studies). However, DTI measures are highly sensitive to partial volume averaging between different tissues including crossing white matter tracts. This causes Dr to be highly heterogeneous across WM for reasons that are unrelated to myelination. Conversely, the Po measure from DSI or HYDI is relatively insensitive to fiber crossing (Wu et al. 2008) so it is more straightforward to compare Po measurements across brain areas as well as between subjects. Challenges associated with the application of DSI methods includes the large gradients necessary for very high diffusion-weighting, the low signal to noise (and noise bias) in images with high diffusion-weighting, and the long scan times associated with the acquisition of a large number of encoding directions. If Po is the only DSI measure of interest, then the acquisition time may be significantly reduced by only acquiring the data from the single outer shell, which makes the acquisition time more comparable to that of DTI (Hosseinbor et al. 2010).

Conclusions

High b-value and DTI measurements were investigated in a large animal model of dysmyelination and brain development on a clinical MRI scanner. Studies like this are critical for translation of quantitative MRI methods to clinical populations. In this study, dysmyelination caused a decrease in the most restricted diffusion as derived from high b-value measurements and an increase in radial diffusivity and a smaller relative increase in axial diffusivities as derived from tensor-based measurements. The observations are consistent with previous measurements in rodent models of dysmyelination. The specific mechanisms of the diffusion changes – differences in myelin or axons or a combination of

both – are still unclear. Further imaging studies with histopathologic correlation are being performed, which should help to disambiguate the specific mechanisms of diffusion related changes with myelination and axons.

Acknowledgments

References

Alexander AL, Hasan KM, Lazar M, Tsuruda JS, Parker DL. Analysis of partial volume effects in Diffusion-Tensor MRI. Magn Reson Med. 2001; 45:770–780. [PubMed: 11323803]

Assaf Y, Cohen Y. Assignment of the water slow-diffusing component in the central nervous system using q-space diffusion MRS: implications for fiber tract imaging. Magn Reson Med. 2000; 43(2): 191–199. [PubMed: 10680682]

Assaf Y, Ben Bashat D, Chapman J, Peled S, Biton IE, Kafri M, Segev Y, Hendler T, Korczyn AD, Graif M, Cohen Y. High b-value q-space analyzed diffusion-weighted MRI: application to Multiple sclerosis. Magn Reson Med. 2002; 47:115–126. [PubMed: 11754450]

Assaf Y, Basser PJ. Composite hindered and restricted model of diffusion (CHARMED) MR imaging of hyman brain. NeuroImage. 2005; 27:48–58. [PubMed: 15979342]

Assaf Y, Blumenfeld-Katzir T, Yovel Y, Basser PJ. AxCaliber: a method for measuring axon diameter distribution from diffusion MRI. Magn Reson Med. 2008; 59(6):1347–54. [PubMed: 18506799]

Barazany D, Basser PJ, Assaf Y. In vivo measurement of axon diameter distribution in the corpus callosum of rat brain. Brain. 2009; 132(Pt 5):1210–1220. [PubMed: 19403788]

Bar-Shir A, Duncan ID, Cohen Y. QSI and DTI od excised brain of the myelin-deficient rat. Neuroimage. 2009; 48(1):109–116. [PubMed: 19539038]

Baratti C, Barnett AS, Pierpaoli C. Comparative MR imaging study of brain maturation in kittens with T1, T2, and the trace of the diffusion tensor. Radiology. 1999; 210(1):133–42. [PubMed: 9885598]

Basser PJ, Mattiello J, Le Bihan DL. Estimation of the effective self-diffusion tensor from the NMR spin echo. J Magn Reson B. 1994; 103:247–254. [PubMed: 8019776]

Basser PJ, Pierpaoli C. Microstructural and physiological features of tissues elucidated by quantitative-diffusion-tensor MRI. Magn Reson Med. 1996; 111:209–219.

Beaulieu C, Allen PS. Water diffusion in the giant axon of the squid: implications for diffusion-weighted MRI of the nervous system. Magn Reson Med. 1994; 32(5):579–83. [PubMed: 7808259]

Berman JI, Mukherjee P, Partridge SC, Miller SP, Ferriero DM, Barkovich AJ, Vigneron DB, Henry RG. Quantitative diffusion tensor MRI fiber tractography of sensorimotor white matter development in premature infants. NeuroImage. 2005; 27(4):862–71. [PubMed: 15978841]

Ben Bashat D, Ben Sira L, Graif M, Pianka P, Hendler Y, Cohen Y, Assaf Y. Normal White Matter Development From Infancy to Adulthood: Comparing Diffusion Tensor and High b Value Diffusion Weighted MR Images. J Magn Reson Imaging. 2005; 21:503–511. [PubMed: 15834918]

Biton IE, Duncan ID, Cohen Y. q-Space Diffusion of Myelin-Deficient Spinal Cords. Magn Reson Med. 2007; 58:993–1000. [PubMed: 17969109]

Biton IE, Duncan ID, Cohen Y. High b-value q-space diffusion MRI in myrlin-deficient rat spinal cords. Magn Reson Imaging. 2006; 24(2):161–166. [PubMed: 16455404]

Bockhorst KH, Narayana PA, Liu R, Ahobila-Vijjula P, Ramu J, Kamel M, Wosik J, Bockhorst T, Hahn K, Hasan KM, Perez-Polo JR. Early postnatal development of rat brain: in vivo diffusion tensor imaging. J Neurosci Res. 2008; 86(7):1520–8. [PubMed: 18189320]

Budde MD, Kim JH, Liang HF, Russell JH, Cross AH, Song S-K. Axonal injury detected by in vivo diffusion tensor imaging correlates with neurological disability in a mouse model of multiple sclerosis. NMR Biomed. 2008; 21(6):589–97. [PubMed: 18041806]

Callaghan, PT. Principles of Nuclear Magnetic Resonance Microscopy. Clarendon Press; Oxford: 1991.

Cook, PA.; Bai, Y.; Nedjati-Gilani, S.; Seunarine, KK.; Hall, MG.; Parker, GJ.; Alexander, DC. Camino: Open-Source Diffusion-MRI Reconstruction and Processing. 14th Scientific Meeting of the International Society for Magnetic Resonance in Medicine; Seattle, WA, USA. 2006. p. 2759

D'Arceuil H, Liu C, Levitt P, Thompson B, Kosofsky B, de Crespigny A. Three-dimensional high-resolution diffusion tensor imaging and tractography of the developing rabbit brain. Dev Neurosci. 2008; 30(4):262–75. [PubMed: 17962716]

Davis SW, Dennis NA, Buchler NG, White LE, Madden DJ, Cabeza R. Assessing the effects of age on long white matter tracts using diffusion tensor tractography. NeuroImage. 2009; 46(2):530–41. [PubMed: 19385018]

Duncan ID, Griffiths IR, Munz M. 'Shaking pups': a disorder of central myelination in the spaniel dog. III. Quantitative aspects of glia and myelin in the spinal cord and optic nerve. Neuropathol Appl Neurobiol. 1983; 9(5):355–68. [PubMed: 6646343]

Eluvathingal TJ, Hasan KM, Kramer L, Fletcher JM, Ewing-Cobbs L. Quantitative diffusion tensor tractography of association and projection fibers in normally developing children and adolescents. Cereb Cortex. 2007; 17(12):2760–8. [PubMed: 17307759]

Ge Y, Law M, Grossman RI. Applications of diffusion tensor MR imaging in multiple sclerosis. Ann N Y Acad Sci. 2005; 1064:202–19. [PubMed: 16394158]

Griffiths IR, Duncan ID, McCulloch M, Harvey MJ. Shaking pups: a disorder of central myelination in the Spaniel dog. Part 1. Clinical, genetic and light-microscopical observations. J Neurol Sci. 1981; 50(3):423–433. [PubMed: 7196438]

Harsan LA, Poulet P, Guignard B, Steibel J, Parizel N, de Sousa PL, Boehm N, Grucker D, Ghandour MS. Brain dysmyelination and recovery assessment by noninvasive in vivo diffusion tensor magnetic resonance imaging. J Neurosci Res. 2006; 83(3):392–402. [PubMed: 16397901]

Harsan LA, Poulet P, Guignard B, Parizel N, Skoff RP, Ghandour MS. Astrocytic hypertrophy in dysmyelination influences the diffusion anisotropy of white matter. J Neurosci Res. 2007; 85(5):935–44. [PubMed: 17278151]

Henry RG, Shieh M, Amirbekian B, Chung S, Okuda DT, Pelletier D. Connecting white matter injury and thalamic atrophy in clinically isolated syndromes. J Neurol Sci. 2009; 282(1–2):61–6. [PubMed: 19394969]

Henry RG, Oh J, Nelson SJ, Pelletier D. Directional diffusion in relapsing-remitting multiple sclerosis: a possible in vivo signature of Wallerian degeneration. J Magn Reson Imaging. 2003; 18(4):420–6. [PubMed: 14508778]

Hermoye L, Saint-Martin C, Cosnard G, Lee SK, Kim J, Nassogne MC, Menten R, Clapuyt P, Donohue PK, Hua K, Wakana S, Jiang H, van Zijl PC, Mori S. Pediatric diffusion tensor imaging: normal database and observation of the white matter maturation in early childhood. NeuroImage. 2006; 29(2):493–504. [PubMed: 16194615]

Hosseinbor, AP.; Fleming, JO.; Wu, Y-C.; Samsonov, AA.; Alexander, AL. An Accelerated, Alternative Approach for Estimating Zero-Displacement Probability in Hybrid Diffusion Imaging. Proc. ISMRM 18th Annual meeting; Stockholm, Sweden. 2010.

Kim JH, Budde MD, Liang HF, Klein RS, Russell JH, Cross AH, Song SK. Detecting axon damage in spinal cord from a mouse model of multiple sclerosis. Neurobio Dis. 2006; 21(3):626–32.

Miller JH, McKinstry RC, Philip JV, Mukherjee P, Neil JJ. Diffusion-tensor MR imaging of normal brain maturation: a guide to structural development and myelination. AJR Am J Roentgenol. 2003; 180(3):851–9. [PubMed: 12591710]

Miller E, Widjaja E, Nilsson D, Yoon G, Banwell B, Blaser S. Magnetic resonance imaging of a unique mutation in a family with Pelizaeus-Merzbacher disease. Am J Med Genet A. 2010; 152A(3):748–52. [PubMed: 20186781]

Mulkern RV, Gudbjartsson H, Westin C-F, Zengingonul HP, Gartner W, Guttmann CRG, Robertson RL, Kyriakos W, Schwartz R, Holtzman D, Jolesz FA, Maier SE. Multi-component apparent diffusion coefficients in human brain. NMR Biomed. 1999; 12:51–62. [PubMed: 10195330]

Pierpaoli C, Basser PJ. Toward a Quantitative Assessment of Diffusion Anisotropy. Magn Reson Med. 1996; 36:893–906. [PubMed: 8946355]

Nadon NL, Duncan ID, Hudson LD. A point mutation in the proteolipid protein gene of the 'shaking pup' interrupts oligodendrocyte development. Development. 1990; 110:529–537. [PubMed: 1723945]

Nadon NL, Duncan ID. Molecular analysis of glial cell development in the canine 'shaking pup' mutant. Dev Neurosci. 1996; 18:174–184. [PubMed: 8894446]

Ono J, Harada K, Sakurai K, Kodaka R, Shimidzu N, Tanaka J, Nagai T, Okada S. MR diffusion imaging in Pelizaeus-Merzbacher disease. Brain Dev. 1994; 16(3):219–23. [PubMed: 7943607]

Ono J, Harada K, Takahashi M, Maeda M, Ikenaka K, Sakurai K, Sakai N, Kagawa T, Fritz-Zieroth B, Nagai T, Nlhel A, Hashimoto S, Okada S. Differentiation between dysmyelination and demyelination using magnetic resonance diffusional anisotropy. Brain Res. 1995; 671(1):141–148. [PubMed: 7728526]

Ono J, Harada K, Mano T, Sakurai K, Okada S. Differentiation of dys- and demyelination using diffusional anisotropy. Pediatr Neurol. 1997; 16(1):63–6. [PubMed: 9044406]

Sener RN. Pelizaeus-Merzbacher disease: diffusion MR imaging and proton MR spectroscopy findings. J Neuroradiol. 2004; 31(2):138–41. [PubMed: 15094651]

Song SK, Sun S-W, Ramsbottom MJ, Chang C, Russell J, Cross AH. Dysmyelintaion revealed through MRI as increased radial (but unchanged axial) diffusion of water. NeuroImage. 2002; 17:1429–1436. [PubMed: 12414282]

Sun SW, Liang HF, Le TQ, Armstrong RC, Cross AH, Song SK. Differential sensitivity of in vivo and ex vivo diffusion tensor imaging to evolving optic nerve injury in mice with retinal ischemia. NeuroImage. 2006; 32:1195–1204. [PubMed: 16797189]

Sundgren PC, Dong Q, Gómez-Hassan D, Mukherji SK, Maly P, Welsh R. Diffusion tensor imaging of the brain: review of clinical applications. Neuroradiology. 2004; 46(5):339–50. [PubMed: 15103435]

Suzuki Y, Matsuzawa H, Kwee IL, Nakada T. Absolute eigenvalue diffusion tensor analysis for human brain maturation. NMR Biomed. 2003; 16(5):257–60. [PubMed: 14648885]

Takahashi E, Dai G, Wang R, Ohki K, Rosen GD, Galaburda AM, Grant PE, Wedeen VJ. Development of cerebral fiber pathways in cats revealed by diffusion spectrum imaging. 2010; 49(2):1231–40.

Tyszka JM, Readhead C, Bearer EL, Pautler RG, Jacobs RE. Statistical diffusion tensor histology reveals regional dysmyelination effects in the shiverer mouse mutant. NeuroImage. 2006; 29(4):1058–65. [PubMed: 16213163]

Wedeen VJ, Hagmann P, Tseng W-YJ, Reese TG, Weisskoff RM. Mapping complex tissue architecture with diffusion spectrum magnetic resonance imaging. Magn Reson Med. 2005; 54:1377–1386. [PubMed: 16247738]

Wheeler-Kingshott CA, Cercignani M. About "axial" and "radial" diffusivities. Magn Reson Med. 2009; 61(5):1255–60. [PubMed: 19253405]

Wu Y-C, Alexander AL. Hybrid diffusion imaging. NeuroImage. 2007; 36:617–629. [PubMed: 17481920]

Wu Y-C, Field AS, Alexander AL. Computation of Diffusion Function Measures in q-Space Using Magnetic Resonance Hybrid Diffusion Imaging. IEEE Trans Med Imaging. 2008; 27(6):858–865. [PubMed: 18541492]

Zhang Y, Brady M, Smith S. Segmentation of brain MR images through a hidden Markov random field model and the expectation maximization algorithm. IEEE Trans on Medical Imaging. 2001; 20(1):45–57.

Zhang J, Miller MI, Plachez C, Richards LJ, Yarowsky P, van Zijl P, Mori S. Mapping postnatal mouse brain development with diffusion tensor microimaging. NeuroImage. 2005; 26(4):1042–51. [PubMed: 15961044]

Highlights

- A large animal model (*shaking* pups) of brain dysmyelination was studied.

- High b-value diffusion-weighted imaging and Diffusion tensor imaging were used.

- Brain dysmyelination caused a decreased Zero-displacement probability (Po).

- Brain dysmyelination caused an increased radial diffusivity of DTI.

- Control dogs had significant changes of diffusion measures as brain maturating.
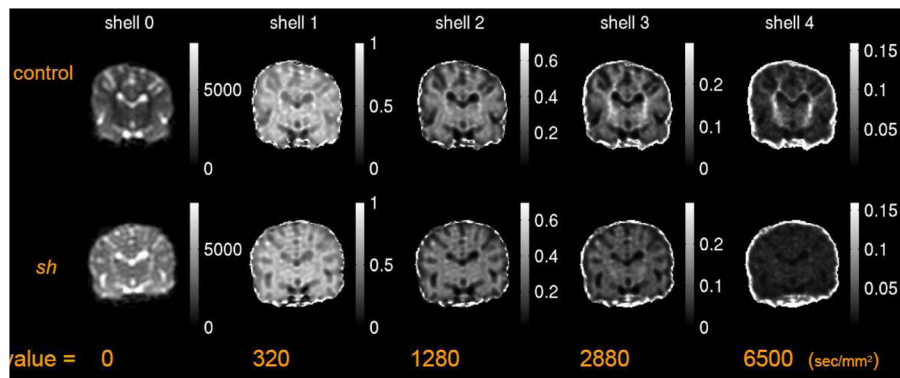
Figure 1.
Geometric means of diffusion-weighted signals at different b-values of HYDI shells of a pair of 3 months old littermate control and *sh* pup. The gray scale at b-value = 0 sec/mm^2 denotes the signal intensity, whereas the gray scale of images with b-value > 0 denotes the ratio of signal intensities to that of b-value = 0 sec/mm^2.
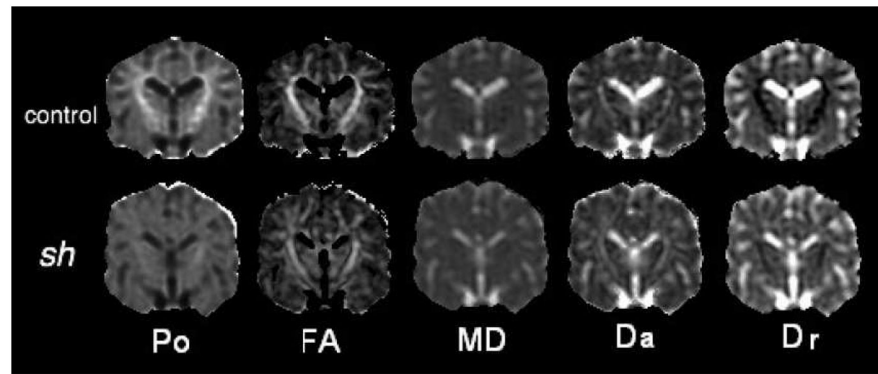
Figure 2.
Maps of diffusion measures of a pair of 3 months old littermate control and *sh* pup.
Notations: Po: zero displacement probability; FA: fractional anisotropy; MD: mean
diffusivity; Da: axial diffusivity; Dr: radial diffusivity.
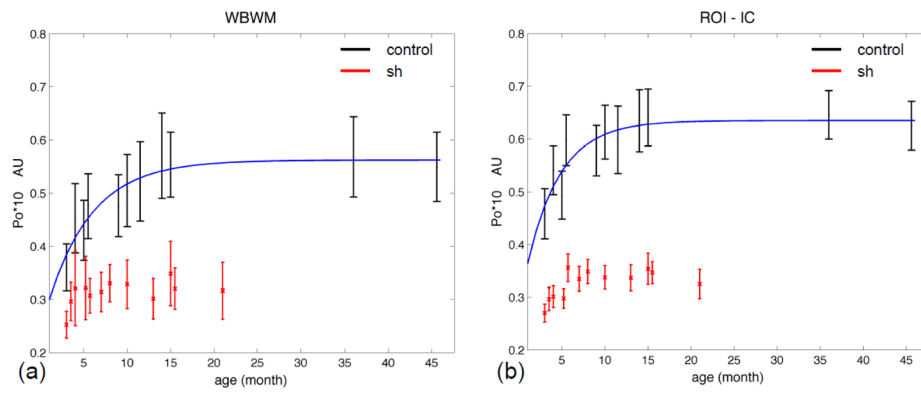
Figure 3.
Po, zero displacement probability, vs. age for the control dogs and *sh* pups. (a) in the whole brain white matter (WBWM). (b) in the region of interest of bilateral internal capsules. (ROI-IC). The control pups had significant nonlinear fit with p-value < 0.05. The fitted lines are in dark blue.
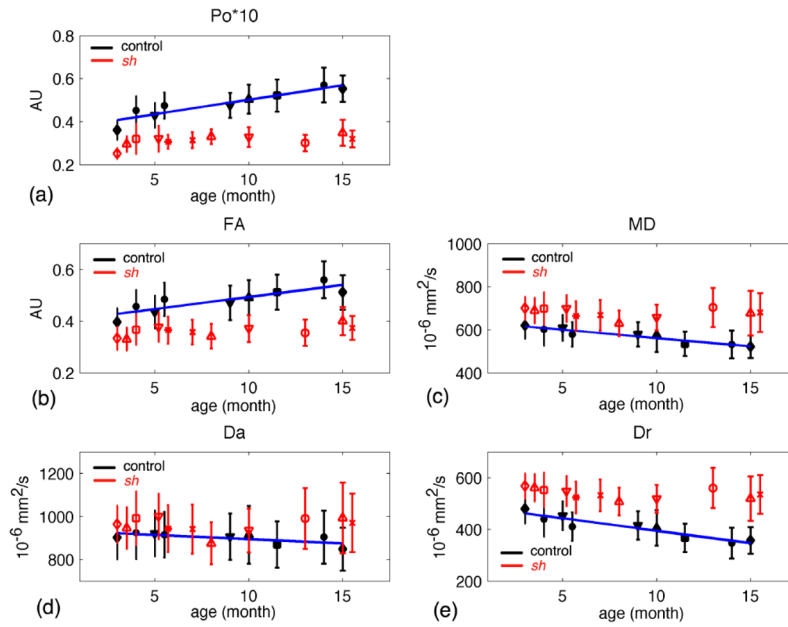
Figure 4.
Diffusion measures in the whole brain white matter (WBWM) vs. age for the control (in black symbols) and *sh* pups (in red symbols). (a) Po, the zero displacement probability; (b) FA, fractional anisotropy; (c) MD, mean diffusivity; (d) Da, axial diffusivity; (e) Dr, radial diffusivity. Only control pups had significant fits (p-value < 0.05), where the regression lines were plotted in dark blue. Each symbol denotes an individual pup.
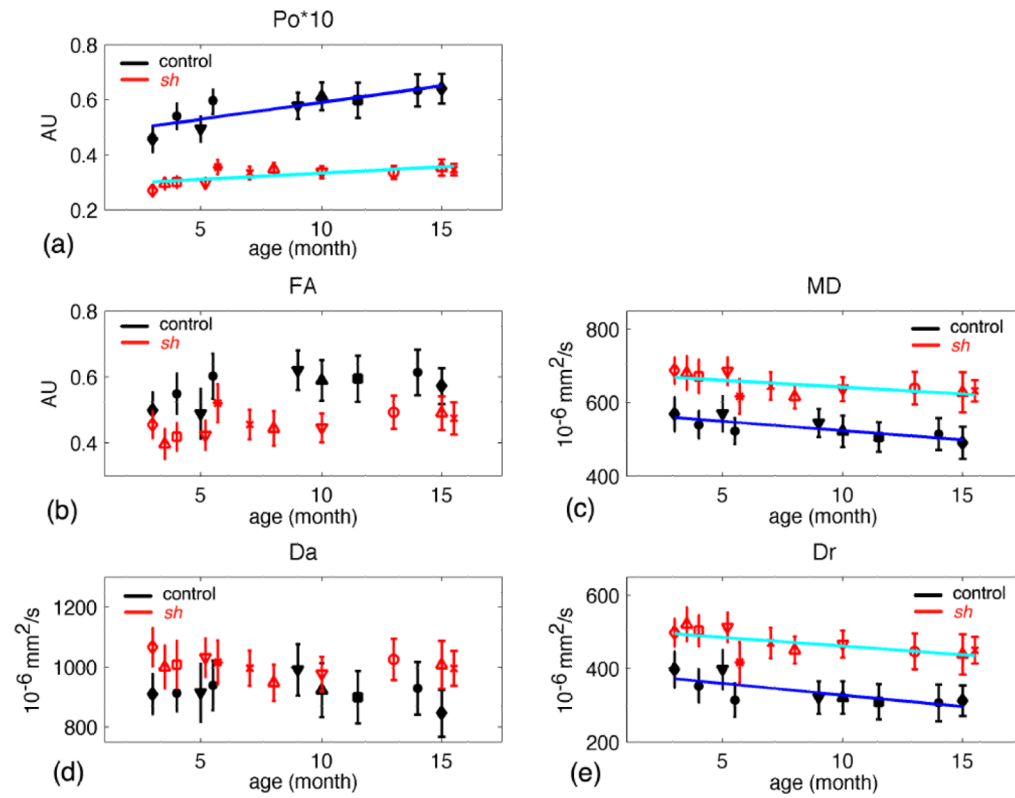
Figure 5.
Diffusion measures in the internal capsules vs. age for the control (in black symbols) and *sh* pups (in red symbols). (a) Po, the zero displacement probability; (b) FA, fractional anisotropy; (c) MD, mean diffusivity; (d) Da, axial diffusivity; (e) Dr, radial diffusivity. Both control and *sh* pups had significant fits (p-value < 0.05) in Po, MD and Dr. The regression lines were plotted in dark blue for the control pups and light blue for the *sh* pups. Each symbol denotes an individual pup.
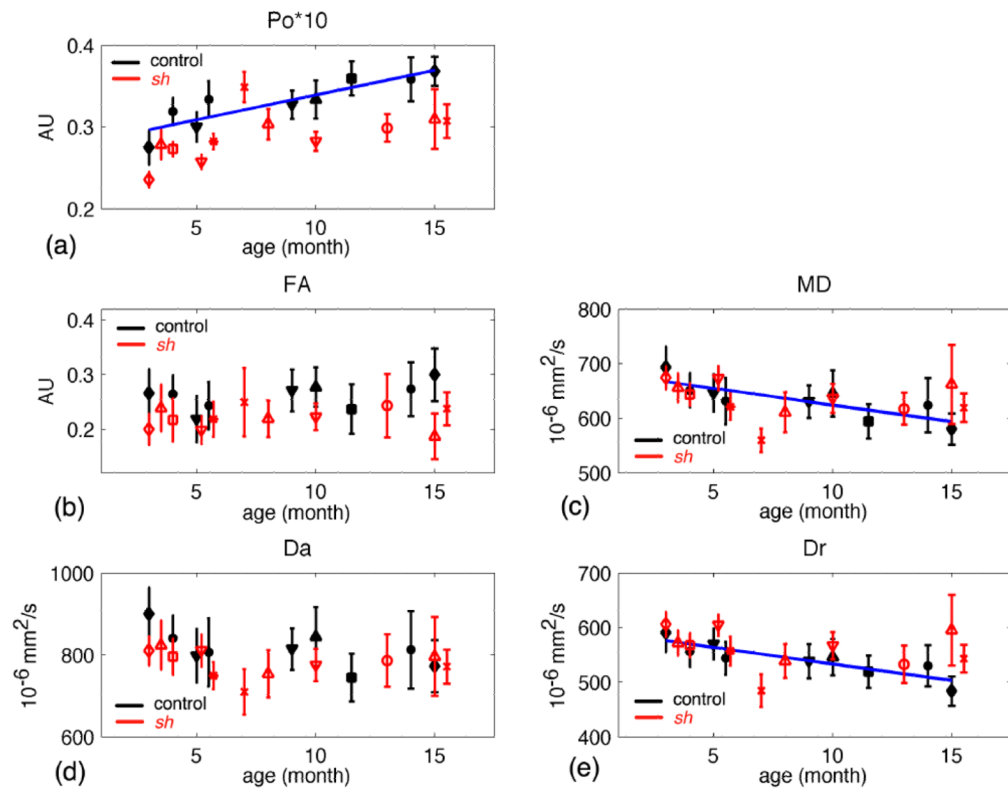
Figure 6.
Diffusion measures in the caudate nuclei vs. age for the control (in black symbols) and *sh* pups (in red symbols). (a) Po, the zero displacement probability; (b) FA, fractional anisotropy; (c) MD, mean diffusivity; (d) Da, axial diffusivity; (e) Dr, radial diffusivity. Only control pups had significant fits (p-value < 0.05) in Po, MD and Dr. The regression lines were plotted in dark blue. Each symbol denotes an individual pup.
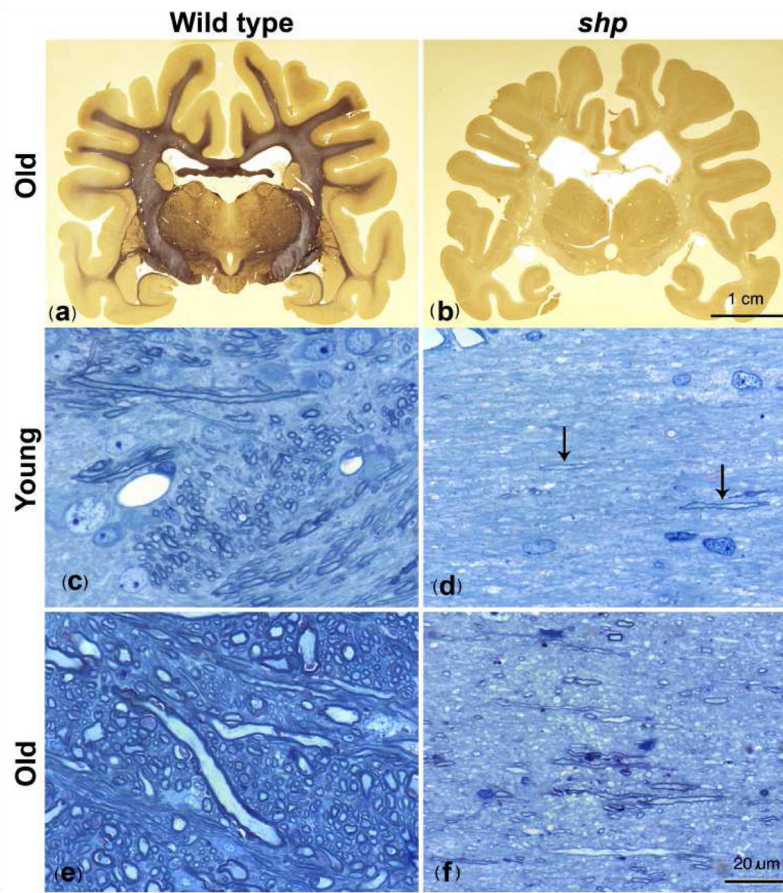
Figure 7.
Light microscopic histology of pup brains. (a), (b) Coronal brain sections from a 2 year old normal dog (a) and a 2 year old shaking pup (b). The mutant brain appears to lack any myelin except some pale staining of parts of the sub-cortical white matter and internal capsule. Higher power images of the internal capsule in a 4 week old normal dog and 5 week old *sh* pup (c, d) and a normal dog at 1 ½ years (e) and shaking pup at 4 months (f) demonstrate normal myelination in wild type (c, e) but a marked paucity of myelin in the mutant (d, f). At 5 weeks in the *sh* pup (d) there are only one or two short stretches of myelin (arrows) whereas at 4 months there are scattered myelin sheaths throughout the neuropil (f) but much less than the normal dog at both time points (c, e). An increase in axon size in the older normal dog (e) compared to the younger dog (c) is evident. (a),(b); Weil stain, 40 μm thick sections Bar = 1 cm, (c)–(f); One micron Toluidine blue stained sections Bar = 20 μm.

Table 1

Hybrid Diffusion Imaging (HYDI) q-space encoding scheme

Shell	Dir. #	b value (sec/mm^2)	q_r (mm^{-1})	Δq_r (mm^{-1})
	1	0	0	
1st	6	320	14.4	14.4
2nd	21	1280	28.8	14.4
3rd	45	2880	43.2	14.4
4th	56	6500	64.9	21.7
	Total	Max	Max	Max
	129	6500	64.9	21.7

Notations: Dir. #: number of diffusion-weighting gradient directions; q_r: radius of HYDI shell in q-space. Δq_r: distance between contiguous shells in q-space.

Table 2

Mean values and standard deviation (sd) of diffusion measures and group differences between controls and *sh* pups using ANOVA test.

		Po	FA	MD (10^{-6} mm²/s)	Da (10^{-6} mm²/s)	Dr (10^{-6} mm²/s)
WBWM	*sh* mean ± sd	0.31 ± 0.02	0.36 ± 0.02	681 ± 22	962 ± 36	540 ± 20
	control mean ± sd	0.50 ± 0.07	0.48 ± 0.05	571 ± 33	900 ± 29	406 ± 43
	diff (%)	**−37.0**	**−25.1**	**19.2**	**6.8**	**33.0**
	p-value	**< 10^{-4}**	**< 10^{-4}**	**< 10^{-4}**	**<10^{-3}**	**< 10^{-4}**
ROI - IC	*sh* mean ± sd	0.33 ± 0.03	0.46 ± 0.04	648 ± 26	1005 ± 30	470 ± 32
	control mean ± sd	0.58 ± 0.06	0.57 ± 0.05	531 ± 25	922 ± 35	335 ± 35
	diff (%)	**−45.0**	**−21.1**	**22.0**	**8.9**	**42.0**
	p-value	**< 10^{-4}**	**< 10^{-4}**	**< 10^{-4}**	**< 10^{-4}**	**< 10^{-4}**
ROI - CN	*sh* mean ± sd	0.29 ± 0.03	0.22 ± 0.02	634 ± 32	781 ± 32	560 ± 34
	control mean ± sd	0.33 ± 0.03	0.27 ± 0.03	642 ± 42	829 ± 53	548 ± 41
	diff (%)	**−13.1**	**−15.5**	−1.2	**−5.8**	2.4
	p-value	**10^{-3}**	**10^{-3}**	0.64	**0.015**	0.42

Number of scans: control: 11 and *sh*: 12; age range from 3 to 45.6 months. The age distributions of the two groups were not significantly different from each other.

diff: the percentage of mean difference to control pup's mean, where "mean difference" is defined as the mean of diffusion measures of the *sh* group minus the mean of the control group.

Bold fonts indicate significant group difference with p-value < 0.05.

Table 3

Results of linear regression analyses of all diffusion measures in the internal capsules (IC) *vs.* age for controls and *sh* pups.
Model: DW-measures = $\beta_0 + \beta_1$*age + noise

		control (df = 7)			*sh* (df = 9)			*sh* – con	
		estimate	p-value	R^2	estimate	p-value	R^2	Estimate difference	p-value
Po	β_0	0.466	**<10⁻⁴**	**0.728**	0.280	**<10⁻⁴**	**0.509**	−0.186	**<10⁻⁴**
	β_1	0.013	**0.005**		0.005	**0.007**		−0.007	**0.046**
FA	β_0	0.512	**<10⁻⁴**	--	0.421	**<10⁻⁴**	--	--	--
	β_1	0.007	0.074		0.004	0.084		--	--
MD	β_0	569	**<10⁻⁴**	**0.686**	680	**<10⁻⁴**	**0.407**	111	**<10⁻⁴**
	β_1	−4.624	**0.012**		−3.767	**0.036**		0.857	0.680
Da	β_0	941	**<10⁻⁴**	--	1022	**<10⁻⁴**	--	--	--
	β_1	−2.561	0.434		−1.900	0.394		--	--
Dr	β_0	386	**<10⁻⁴**	**0.576**	513	**<10⁻⁴**	**0.412**	127	**<10⁻⁴**
	β_1	−5.810	**0.022**		−4.820	**0.017**		0.990	0.707

The last column (*sh* -con) is the comparison of estimates in the linear model between the *sh* pup group and control group using ANOVA. Bold fonts indicate significant fit with p-value < 0.05. The age of pups range from 3 to 16 months.